Unsteady Aerodynamics of Aircraft Maneuvering at High Angle of Attack

Kenneth E. Wurtzler and Robert F. Tomaro
Air Force Research Laboratory/Air Vehicles Directorate
WPAFB, OH

Abstract

The focus of this project is the utilization of an unstructured, parallel CFD flow solver to predict the unsteady aerodynamics acting on fighter configurations maneuvering at high angles of attack. Emphasis is centered on the routine application of analysis methods (grid generation, flow solver, data visualization) to obtain accurate and timely results. An F-18C and F-16C were modeled separately and grids of 6.9 million and 4.5 millions tetrahedral cells respectively were constructed around the aircraft. Viscous, turbulent solutions of each aircraft at various static angles of attack have been completed and are presented. The flight conditions are Mach = 0.25 and angles of attack = 10^o, 20^o, 30^o, 35^o, 40^o, 45^o, 50^o, 55^o, and 60^o. The results reveal vortex paths and the vortex breakdown location at the higher angles of attack and the subsequent loss of lift for the aircraft. Initial time-accurate computations at selected angles of attack highlight the unsteadiness of the localized flow. Future time-dependent pitching analyses will be accomplished and the results compared to these static results.

Introduction

The state of the art in numerical simulation of aircraft is generally limited to steady-state analysis of complete aircraft or unsteady analysis of simple geometries or aircraft components. Grid generation and geometry modeling has matured to the point where aircraft with weapons and detailed geometric complexity can be modeled. Further advancement to an analysis of viscous, unsteady aerodynamics of a complete aircraft requires large amounts of computer time due to the large number of grid points and the slow advancement of the solution process.

Research into the area of high angle of attack aerodynamics has been dominated by experimental testing. Wind tunnel tests have been used initially to investigate the impact of different forebody shapes on the vortical flow field structure shedding from the nose. Traditional fighter forebody shapes of a slender nose (F-15, F-18) as well as newer, sharp-edged forebodies (F-117) were evaluated. Additional research attempted to control the shedding vortices for optimal aerodynamic benefit. With flight envelopes being expanded due to changing tactics and engineering ability, fighter aircraft were designed and expected to fly at higher angles of attack and maintain directional control. However, while pitching to high angles of attack, the vertical tails become surrounded by turbulent, dead air and are limited in their directional control capability. Therefore, relatively small side forces on the nose, even at zero sideslip, can dominate directional stability, creating large yawing moments. These small side forces

are a result of asymmetrical shedding of the forebody vortices. Small surface imperfections such as radome gaps, dents, and sharp paint depth mismatches can affect the strength and path of one of the vortices. The resultant net side force can then increase and the flow becomes unstable. This condition of aircraft experiencing severe yawing moments at high angle of attack flight is called nose-slice departure. It is an unsteady phenomenon and can be catastrophic.

After this discovery, the research emphasis shifted to finding actions and procedures that could prevent or lessen the asymmetry or even manipulate the flow for directional control. Geometric or passive flow control treatments, such as strakes and vanes, were evaluated as were pneumatic or active flow control techniques, consisting of blowing and suction. The majority of this work was either wind tunnel experiments or flight tests. Tunnel experiments validated basic concepts and ideas but were limited to sub-scale models and simple geometries. NASA managed the High Alpha Research Vehicle Program (HARV) which utilized an F-18 aircraft with geometric forebody modifications for better control at high angle of attack flight. The Air Force conducted pneumatic experiments on the X-29 aircraft with a similar objective of forebody vortical flow control. Both programs were supported by wind tunnel tests of innovative ideas and techniques. The overall result of these two programs was that the ability to maintain directional stability at high angles of attack was possible with both geometric and pneumatic techniques. However, these results were just for each individual aircraft and could not be generalized. Also, since these programs just focused on the aerodynamic result, issues dealing with system integration and fleet modification were to be resolved by each operational command.

Computational research has been mainly focused on a basic understanding of vortical flows shedding from simple geometries such as ogive cylinders, bodies of revolution, and wing/fuselage shapes. Previous computer resource limitations constrained these investigations to steady-state flow and fixed angles of attack. The majority of the research centered on what is needed in a flow solver to accurately capture the vortical flows. Since the vortex shedding from a slender forebody is viscously dominated, a Navier-Stokes flow solver is needed to accurately capture the resulting flow. However, for sharp-edged geometries, an Euler flow solver is adequate to simulate the flow since the creation of the vortices is caused by the sharp edge. The cumulative result of this work was that computational analysis was capable of capturing the physics of forebody vortical flows and could predict vortex asymmetry from geometric disturbances.

As the technology pushed towards controlling the forebody vortices for directional control, the computational research community followed with analysis of both passive and active flow control methods. Specifically, the Applied CFD Section investigated both geometric [1] and pneumatic flow control [2] methods on the Air Force Fighter Lift and Control (FLAC) Program. With the FLAC being a sharp-edged forebody, Euler methods were used to simulate the flow. Strake sizing and placement were investigated, as were various pneumatic blowing coefficients. Comparisons with wind tunnel results were in good agreement. For slender forebody shapes, a fully viscous analysis is required which increases grid points and needed computer time. This limited analysis capability to aircraft components and simple aerodynamic flows. Current research in the Applied CFD Section is focused on the computational analysis of the F-15 forebody at high angles of attack [3]. A wind-tunnel analysis of surface imperfections and the addition of various strakes to the forebody was conducted to assess

possible flow control methods. The computational analysis utilized *Cobalt*$_{60}$ to compute the forebody vortices and impact of surface imperfections and vortex control methods. Comparisons to wind tunnel results showed very good agreement and concluded the applicability of numerical methods to successfully model the asymmetrical vortex shedding and flow control methods. The work described in this paper is the logical follow-on to the above work.

Technical Approach

The technical approach involves the seamless application of grid generation, flow solver, and data visualization. Grid generation was accomplished with the code VGRIDNS from NASA Langley. Flow solutions were calculated using *Cobalt*$_{60}$. Flow visualization was achieved using FieldView. The first phase of the project consisted of steady-state calculations at a range of angles of attack from 10^o through 60^o. Subsequent to that, time-accurate calculations were obtained at the static angles 40^o and 55^o. These are compared to the steady state cases to see how the vortex breakdown location is impacted by unsteady flow.

The use of an unstructured grid allows great detail to be maintained on the model. Combined with parallel technology, larger problems can be calculated in a shorter time period. The F-18C grid consists of 6.9 million tetrahedral cells with 3.8 million of those cells in the boundary layer. The subsequent y+ was 3.4. The aircraft was modeled with wing pylons and wingtip rail launcher. The inlet and exhaust were each modeled with the corresponding flow. Details of the modeling of the wing pylons and boundary layer diverter are shown in Figure 1. The F-16C grid consists of 4.5 million tetrahedral cells with 2.3 million of those cells in the boundary layer. The average y+ is 1.8. The inlet was modeled to the engine face. The nozzle was modeled with a flat exhaust plane at the edge of the actual nozzle. The entire F-16C grid generation process (geometry acquisition to complete volume grid) took 2 weeks using VGRIDNS. A second grid was obtained by combining the tetrahedral in the boundary layer into prisms. This reduced the number of boundary layer cells by 2/3 while maintaining boundary layer spacing. Figure 2 shows the forward fuselage and the vertical tail modeled with all antennae shapes intact. Previous structured grid generation methods would have required a 5-times increase in grid construction time for similar detail retention in both cases.

Flight conditions used for these calculations were Mach = 0.25, altitude = sea level. All cases were run with the Spalart-Allmaras turbulence model. Timing information for the F-16C 45^o case is as follows: 60 processors, grid partitioned in 545 seconds, 32 sec/iterations (7.1 μsec/cell/iteration).

Methodology

Cobalt$_{60}$ is a parallel, implicit unstructured Euler/Navier-Stokes flow solver. The code is CHSSI CFD-2. *Cobalt*$_{60}$ accepts arbitrary cell types and allows a variety of cell types in a single grid. The finite-volume, cell-centered solver is based on the exact Riemann solver of Godunov. A more efficient Riemann solver based on the iterative method of Gottlieb and Groth is utilized.

Second-order spatial accuracy is achieved through a least squares reconstruction of the primitive variables. The least squares influence matrix is composed of the unknown coefficients of a second-order accurate Taylor series using the nearest neighbors of the current cells as a stencil. This method approximates a "central-differenced" gradient at the cell face. In general, the influence matrix is over-specified since the current cell has more neighboring cells than unknown coefficients. Thus, the "fit" of the data with the minimum L_2 norm error is solved for by a QR factorization. The QR factorization is chosen over an LU elimination because of its greater stability, which is important on high aspect ratio viscous meshes. In general, the face values must be limited so as to be non-extremal. Limiting is an important task, as stability of the method is required without being overly dissipative, thereby negating the advantage of the second-order scheme over the first order scheme. The limiting employed in *Cobalt*$_{60}$ is based on a one sided gradient for a fully upwind cell [4]. The formulation of the viscous terms is required to possess two attributes: it must be conservative and it must satisfy the discrete maximum principle. Conservation is easily satisfied by constructing viscous fluxes at each face and ensuring those fluxes are applied to both cells sharing any given face. Satisfying the discrete maximum principle is achieved by first constructing the tangential components of the gradient vector. The normal component is constructed as a function of the cell centroid values and the tangential component. Turbulent solutions are obtained using the Spalart-Allmaras turbulence model.

Implicit integration schemes are unconditionally stable, and therefore allow an arbitrary time step to be taken. Realistically, there is a physical time step limit for each unsteady case. If this time step limit is violated, the algorithm will provide answers but will miss some of the important unsteady flow characteristics. This limit depends on the time scales of the unsteady flow phenomena being simulated. The implicit temporal integration scheme was reported by Tomaro *et al* [5]. Second-order temporal accuracy is achieved by a one point backwards Taylor series expansion in time. *Cobalt*$_{60}$ employs a cell-by-cell implicit scheme including both the analytical inviscid and viscous Jacobians, thereby linearizing the governing equations. The inviscid Jacobians are based on van Leer's flux vector splitting to accurately capture the flow propagation. The viscous Jacobians are implemented for robustness of turbulent solutions and are split on a simplified eigenvalue approach. The implicit algorithm couples the flow equations and allows for faster convergence rates. Typically, steady-state solutions are converged under 2,000 iterations. The coupled equations create an influence matrix for each cell that must be inverted. This is accomplished by be employing a LU decomposition on the matrix equation resulting in a Gauss-Seidel iterative scheme. Multiple matrix sweeps can be employed to obtain a better solution to the linearized equations. A Newton sub-iteration method is utilized to better converge each time step in an unsteady problem, thereby allowing larger time steps.

Parallelization Issues

The original serial version of the flow solver, which was written in FORTRAN 77, was first rewritten in Fortran 90 to take advantage of the new features available in the language. For example, all work arrays are allocated at runtime, eliminating the need to recompile the code for different grids/problems. This also makes it possible to reduce memory requirements when the user requests simpler physics or numerics. Array syntax and array operations replace do loops where appropriate, making the code more readable. Global variables are defined in modules, replacing many named common blocks, and a

single easy-to-change parameter was defined to globally set the code to single- or double-precision numerical accuracy. Overall, using Fortran 90 significantly improves software modularity and maintainability and makes it possible to use one source code for all parallel platforms.

Parallelization follows the domain decomposition paradigm where each processor operates on a subsection (zone) of the original grid. The Message Passing Interface (MPI) library is used to pass information between processors. Various MPI features, such as non-blocking communications, persistent communication requests, and vector/indexed MPI datatypes are used to minimize the communications overhead. Considerable care was taken to ensure the zonal boundaries are computed in exactly the same manner as the zonal interiors. At zonal boundaries, the conserved variables for each boundary cell, the initial conditions for the Riemann problem for each boundary face and the gradients in each boundary cell (viscous cases only) are passed to the neighboring zones (processor). Additionally, the implicit time integration scheme requires the communication of boundary cell residual data during each sweep of the iterative matrix solver. Since the Jacobi method uses residuals from the previous sweep only, these residuals are communicated at the end of each sweep. The symmetric Gauss-Seidel method, however, uses the latest residuals as they become available. Technically, then, the residuals of zonal boundary cells should be communicated to neighboring zones (processors) immediately upon their calculation. However, we have found that passing the zonal cell residuals at the end of each sweep works very well with the Gauss-Seidel method. This introduces some Jacobi character at the zonal boundaries, which theoretically slows the convergence rate for multi-zonal (parallel) cases. However, we have experienced virtually no degradation in convergence rate, certainly because the interface sizes have been kept relatively small. Even if a noticeable degradation in convergence were to exist, additional sweeps and/or additional Newton sub-iterations would remove the problem. A discussion of these two zonal boundary treatments is given in Grismer [6].

The major unstructured grid-generation systems that we use, VGRIDns and TETMESH [7], create single-zone meshes exclusively. Therefore, the Parallel METIS domain decomposition library of Karypis and Kumar [8,9], has been directly incorporated into the flow solver to divide the grid into nearly equally sized zones that are then distributed one per processor. Care is taken to evenly distribute the storage requirements of the original, single-zone grid across all the processors during this process. This maintains the memory scalability of the code; i.e. adding more processors increases the size of the problem that can be solved. METIS is used because of its demonstrated performance in the rapid generation of nearly equally balanced zones (based on cell number) with minimal interface size. The flow solver is then very well load-balanced with little communication overhead, explaining its scalability as described below. Details about the multi-level recursive bisection techniques used by METIS, as well as its performance versus other methods, are contained in [8].

A schematic of how *Cobalt*$_{60}$ is incorporated into the parallel computing environment is shown in Figure 3. The thinking behind this integration is to be as flexible and robust as possible in the computing environment. Figure 4 indicates the scalability of the code on three different architectures, an IBM SP2, Cray T3E, and an SGI Origin2000. Both figures show the speedup obtained over one processor versus the number of processors for a given problem. The benchmark problem considered is a three-dimensional, inviscid flow ($M_\infty = 0.85$) over an arrow-wing body configuration, modeled with 435,000

tetrahedra. The ideal line represents perfect scalability. The "superscalability" is the result of improved cache performance on each processor as the size of the grid zones decreases. The randomness of unstructured grids results in poor cache utilization: a byproduct of partitioning the grid is better data locality and therefore improved cache performance.

HPCMP Resources

The computations achieved during this project were acquired using the Maui HPCC (MHPCC) IBM SP2 and the NAVO T3E. For FY99, this project had 236,000 hours assigned for the MHPCC IBM SP2 and 250,000 hours for the NAVO T3E. The hours on the T3E were subsequently reduced to 150,000 as a result of limited access during the first several months of the project. The current and past rate of usage is shown in Figure 5.

Findings/Insights

The initial phase of this project is to define the vortex paths and breakdown positions for both the F-16C and F-18C aircraft at several static angles of attack. For an aircraft performing a pitch-up maneuver, the data from these static cases can provide a basis for understanding the physical parameters of the flow. Lift data can be used to help locate the angle of attack where the vortex breakdown negatively affects the aircraft's lift. A plot of C_L versus angle of attack for both the F-16C and F-18C is shown in Figure 6. The linear relationship between lift and angle of attack is maintained up to about 35^o for both aircraft. After this point, there is degradation in lift that occurs when the lex (leading edge extension) vortex breakdown position comes forward over the wing. This breakdown region is characterized by a stagnation region and reverse flow. The breakdown point location is dependent on the correct modeling of the turbulence. For these cases, the Spalart-Allmaras turbulence model is deemed adequate. Further modifications will incorporate vortex specific terms and this will be evaluated as to its effectiveness.

Each grid had grid clustering along the pre-supposed vortex path coming off of the lex. The forward views of each aircraft have fuselage cuts with color contours of vorticity magnitude. The scale is maintained constant for each case. The streamlines are used to portray the vortex core and breakdown regions. The straight portion of the streamlines represents the core of the vortex, where there is some downstream flow direction maintained. A stagnation point with reverse flow behind it characterizes the breakdown location. The streamlines then become somewhat less capable of identifying vortex parameters due to the instability of the region.

The F-16C geometry consists of a rounded forebody with a leading edge extension joining the forebody with the wing. The separation off of the forebody is viscous-dominated while the separation off of the sharp lex is geometry-dominated. Therefore, the separation point for the forebody will vary according to flight conditions while the separation point off the lex will remain relatively constant. A qualitative evaluation of the flowfield is represented in Figures 7-10 for the F-16C. The main vortex coming off of the F-16C lex at 30^o angle of attack remains intact until mid-wing. The forebody vortices, which can

contribute to yawing instability at the nose, begin to develop after 30^o and are entrained by the lex vortex past the cockpit. This entrainment moves forward as the angle of attack increases. The forebody vortex begins to move off the sides of the body and separates more towards the centerline. At the higher angles of attack, the burst location of the lex vortex moves forward until at 60^o the flow is almost totally reverse. Figure 11 shows the burst region and how the location and breakdown dynamics change due to higher angles of attack. The lower angle of attack breakdown is more controlled and 'stable' than at the higher angle of attack.

The F-18C differs from the F-16C in many ways. The F-18C is larger, has two engines, each with it's own intake, and has twin vertical tails. However, both aircraft have rounded forebodies and have leading edge extensions coming off of the forebodies. Therefore, the flow patterns for two aircraft are similar but their impact on each individual aircraft will be different. A qualitative evaluation of the flowfield is represented in Figures 12-15 for the F-18C. At 30^o, the lex vortex remains strong and coherent until past the wing. The secondary lex vortex runs the length of the lex and is swept out along the wing leading edge. As the angle of attack increases, the burst location of the lex vortex moves forward until at 60^o, the vortex region is domination by a reverse flow direction. The forebody vortices remain on the body and are swept onto the lex at a more forward location at the higher angles of attack.

This static data will be compared to unsteady data at a fixed angle of attack and to unsteady data from a prescribed pitch motion. This will be accomplished towards the end of the first year of the project. From this steady data at a fixed angle of attack, the flowfields for both the F-16C and F-18C have been identified. The forebody geometry will then be modified to produce a flow asymmetry and the aircraft will be put through a controlled pitch maneuver.

Acknowledgements

The work mentioned in this paper was supported by the efforts of the following people: Matt Grismer, Don Kinsey, William Strang, Hugh Thornburg, and Frank Witzeman. The ASC MSRC provided assistance with the video display of data.

References

1. Wurtzler, K., "Numerical Analysis of a Chined Forebody with Asymmetric Strakes," AIAA 93-0051, January 1993.
2. Wurtzler, K., "Numerical Analysis of a Chined Forebody with Asymmetric Blowing," AIAA 94-0171, January 1994.
3. Wurtzler, K., "An Effectiveness Study of F-15 Forebody Flow Analysis Using $Cobalt_{60}$," AIAA 99-0536, January 1999.
4. Strang, W.Z., Tomaro, R.F., and Grismer, M.J., "The Defining Methods of *$Cobalt_{60}$*: A Parallel, Implicit, Unstructured Euler/Navier-Stokes Flow Solver," AIAA 99-0786, January 1999.
5. Tomaro, R.F. and Strang, W.Z., "An Implicit Algorithm for Solving Time Dependent Flows on Unstructured Grids," AIAA 97-0333, January 1997.

6. Grismer, M.J., Strang, W.Z., Tomaro, R.F., and Witzeman, F.C., *"Cobalt$_{60}$*: A Parallel, Implicit, Unstructured Euler/Navier-Stokes Solver." *Advances in Engineering Software*, Vol. 29, No. 3-6, pp.365-373, 1998.
7. Pirzadeh, S., "Three-Dimensional Unstructured Viscous Grids by the Advancing-Layers Method," *AIAA Journal*, Vol. 34, No. 1, January 1996, p.43-49.
8. Karypis, G. and Kumar, V., *METIS Unstructured Graph Partitioning and Sparse Matrix Ordering System Version 2.0*. University of Minnesota, Department of Computer Science, Minneapolis, MN 55455, August 1995.
9. Karypis, G., Schloegel, K. and Kumar, V., *ParMETIS: Parallel Graph Partitioning and Sparse Matrix Ordering Library Version 1.0*. University of Minnesota, Department of Computer Science, Minneapolis, MN 55455, July 1997.

Figures

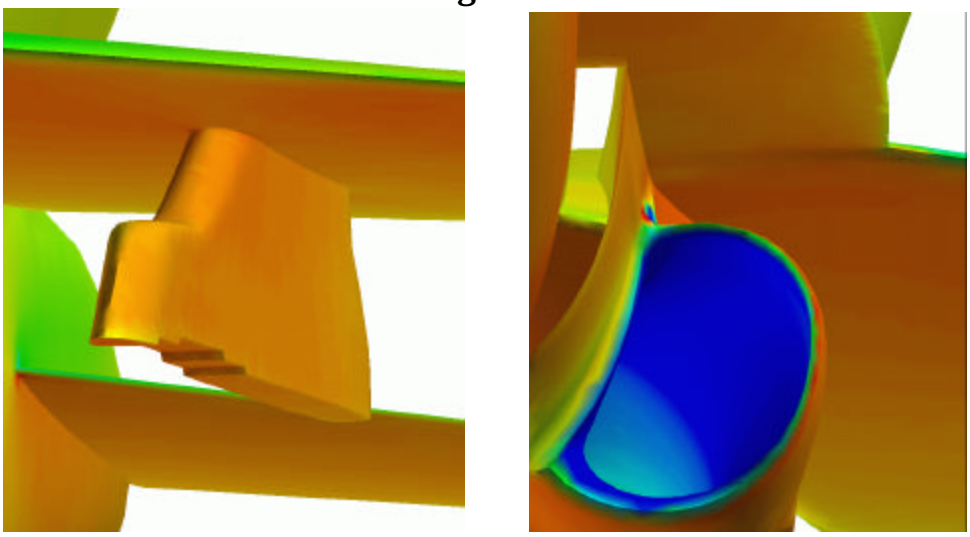

Figure 1. Close-up of F-18C geometry showing wing pylon and boundary layer diverter at inlet.

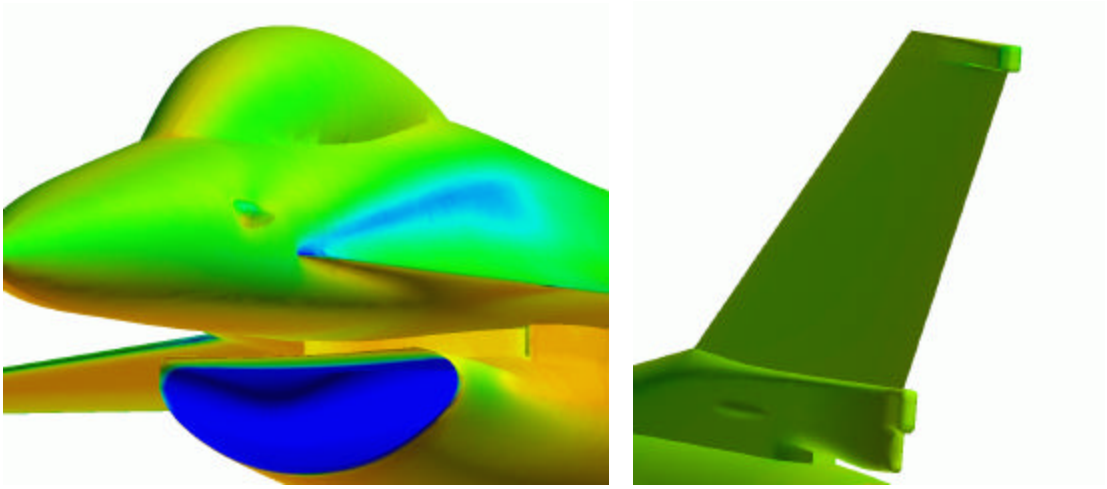

Figure 2. Close-up of F-16C geometry showing forward fuselage and vertical tail.

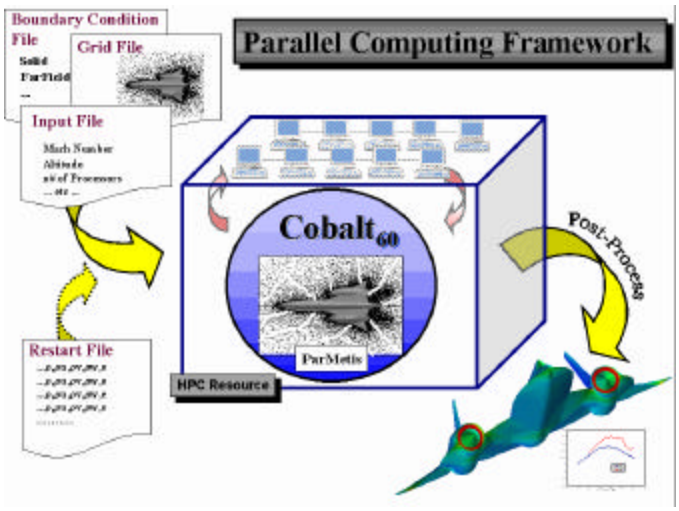

Figure 3. Schematic of *Cobalt*$_{60}$ implementation into a parallel computing environment.

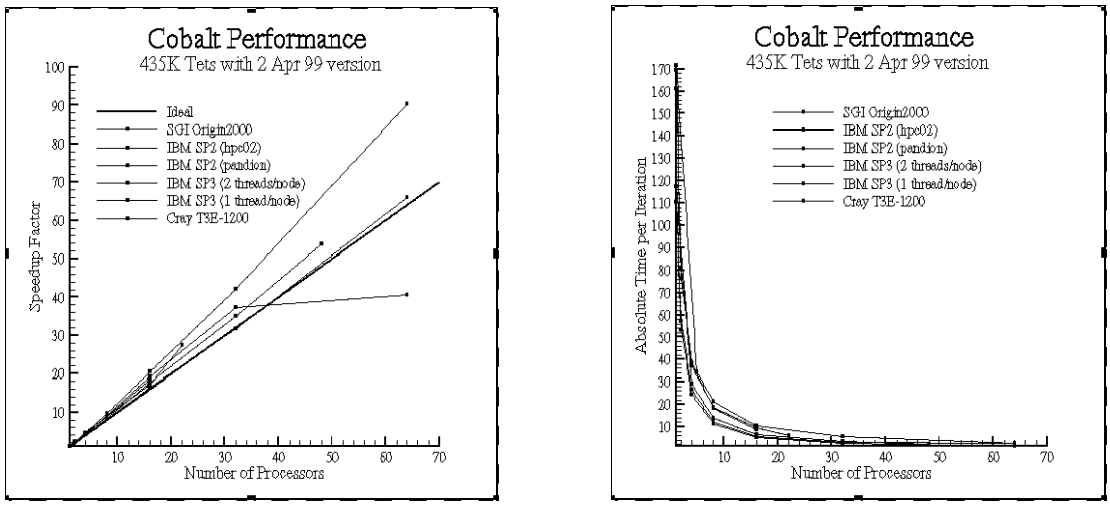

Figure 4. Parallel speed-up for 435,000 cell tetrahedral grid achieved on 3 different architectures.

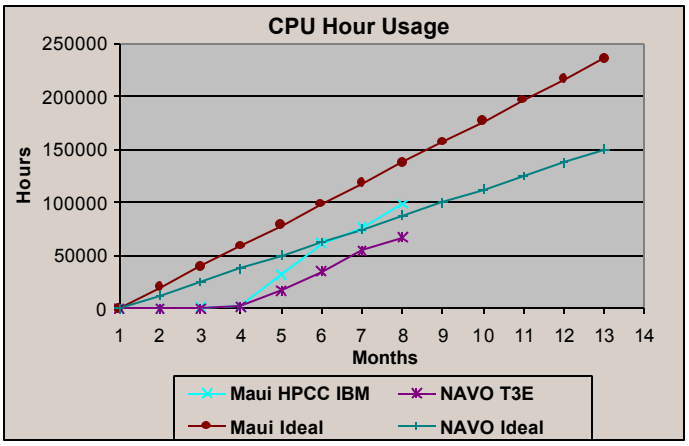

Figure 5. Utilization of hours on Maui IBM SP2 and NAVO T3E.

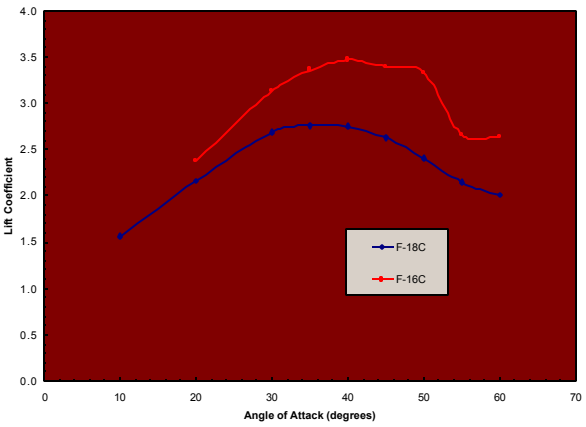

Figure 6. C_L vs. Angle of Attack for the F-18C and F-16C.

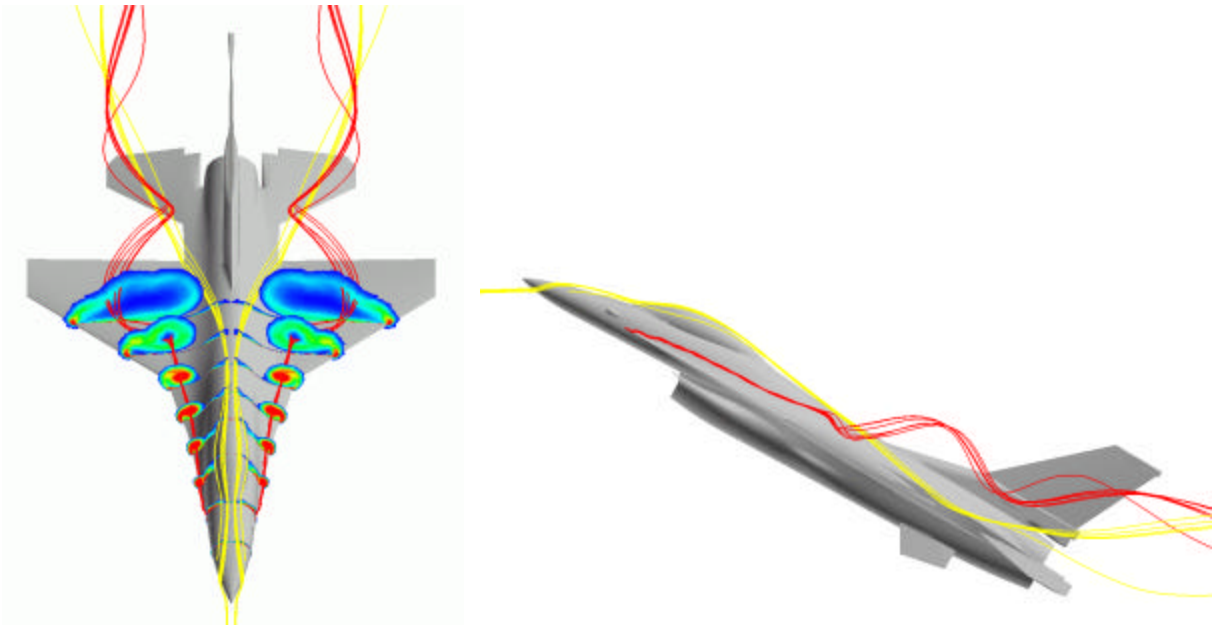

Figure 7. F-16C at 30^{o} angle of attack. Surface cuts on top view are of vorticity magnitude. Red streamlines represent lex vortices and yellow streamlines represent forebody vortices.

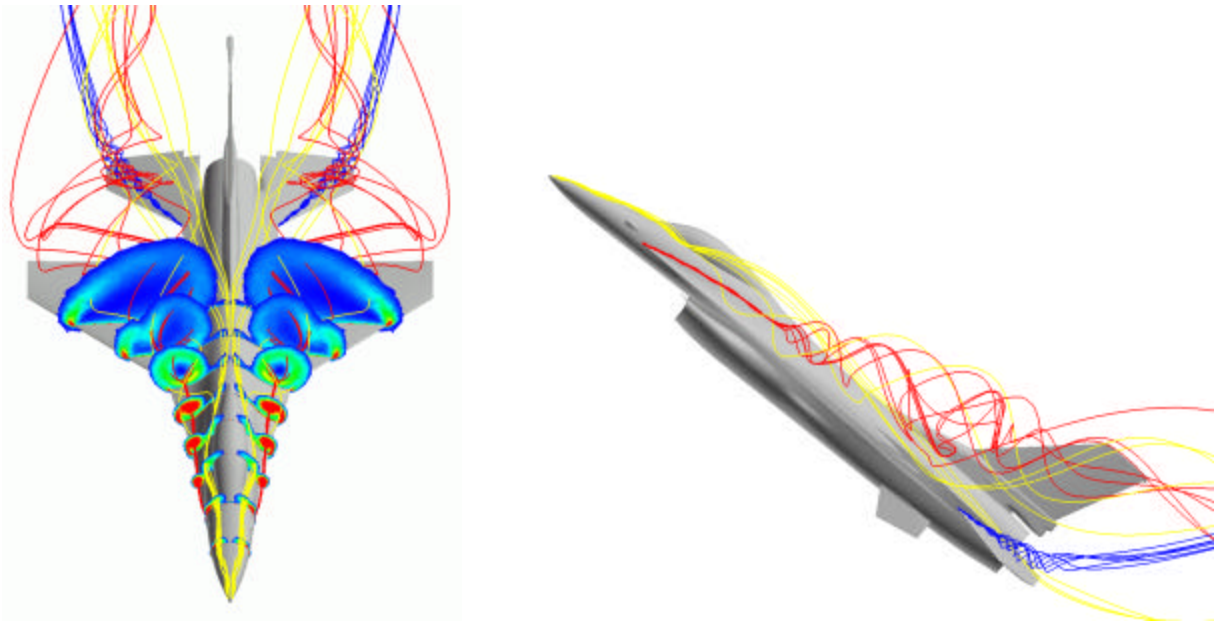

Figure 8. F-16C at 40^{o} angle of attack. Surface cuts on top view are of vorticity magnitude. Red streamlines represent lex vortices, yellow streamlines represent forebody vortices, and blue streamlines represent horizontal tail vortices.

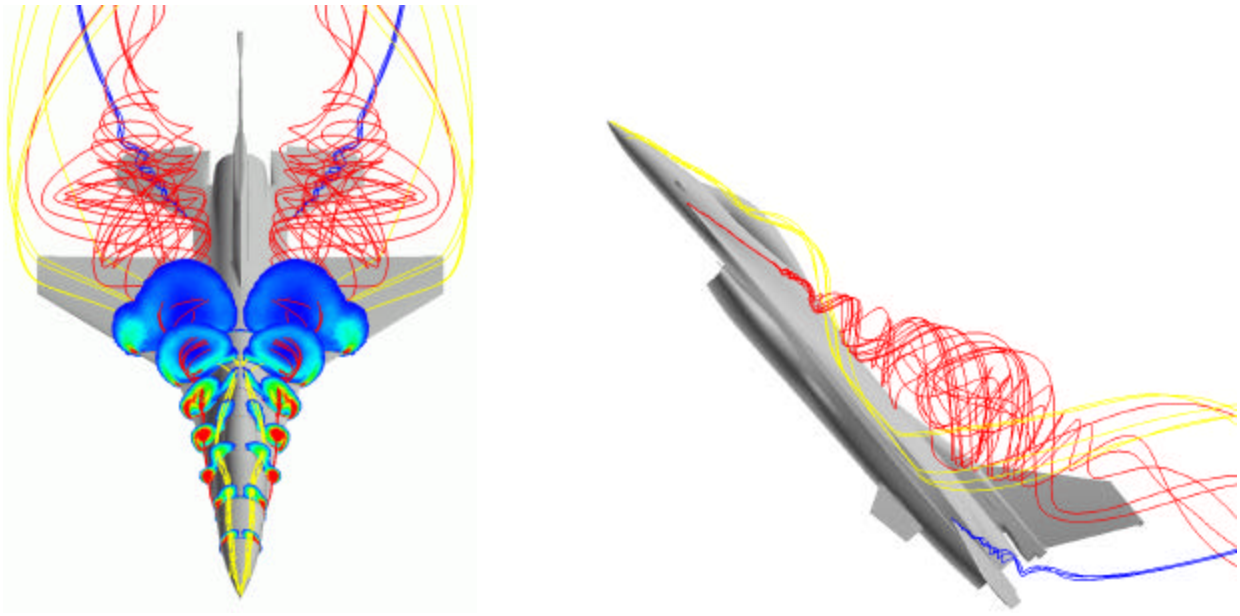

Figure 9. F-16C at 50^{o} angle of attack. Surface cuts on top view are of vorticity magnitude. Red streamlines represent lex vortices, yellow streamlines represent forebody vortices, and blue streamlines represent horizontal tail vortices.

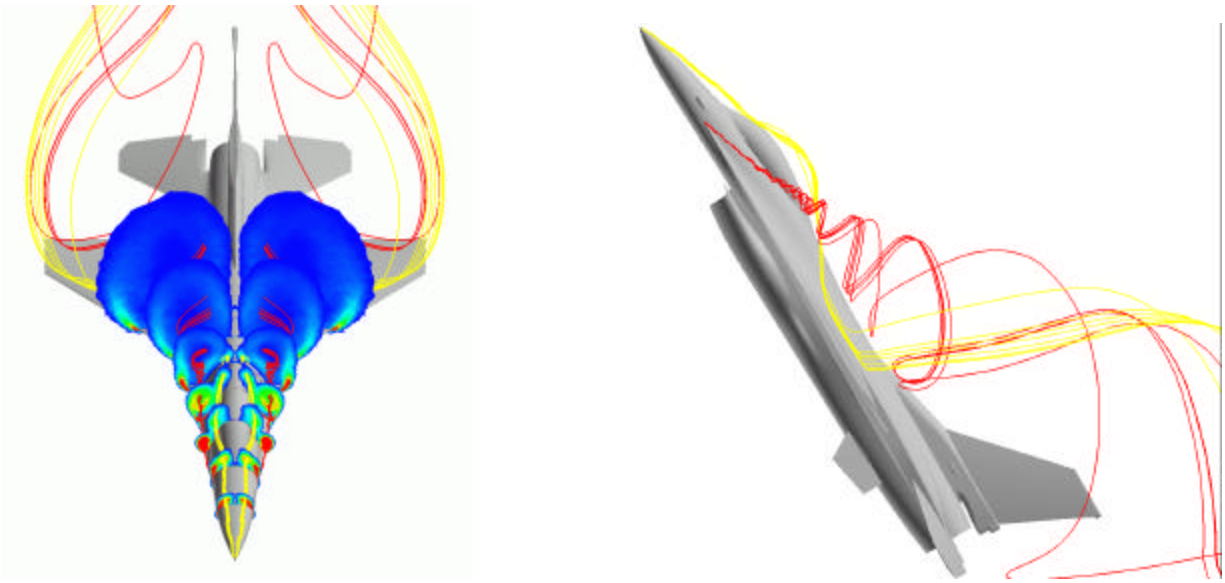

Figure 10. F-16C at 60^{o} angle of attack. Surface cuts on top view are of vorticity magnitude. Red streamlines represent lex vortices and yellow streamlines represent forebody vortices.

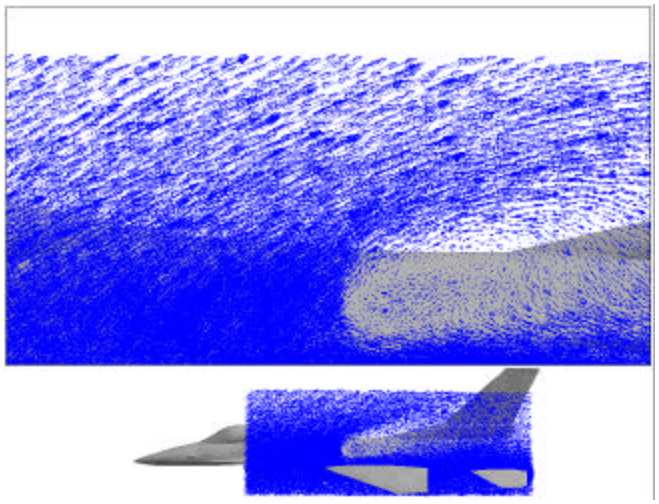

a

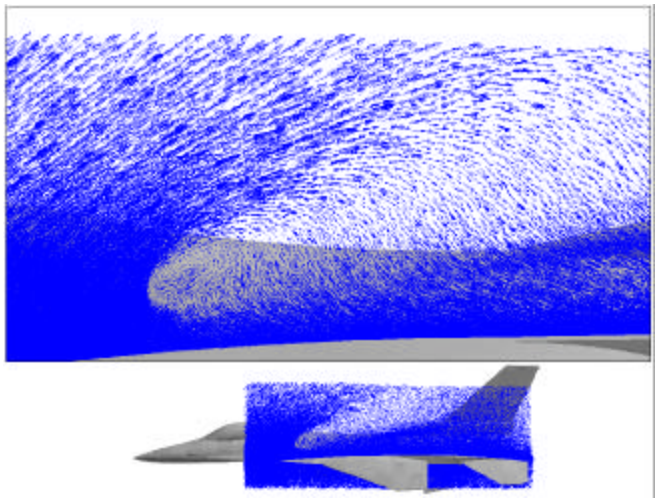

b

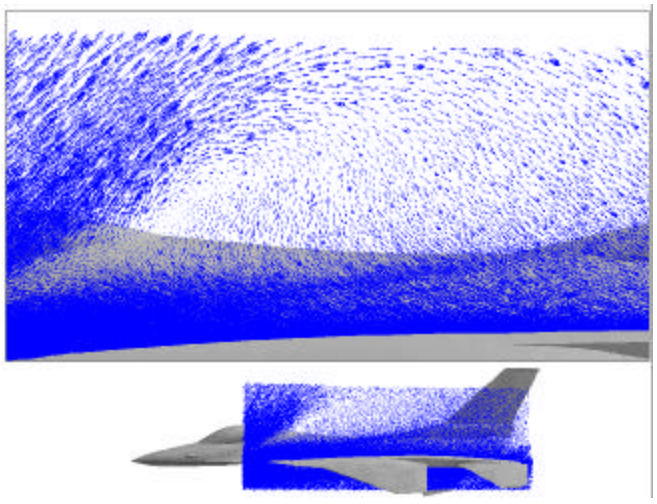

c

Figure 11. Vertical cut plane through center of vortex burst region with vectors of velocity projected onto plane. Breakdown point show in expanded region. Angle of attack a)30^{o} b)45^{o} c)55^{o}.

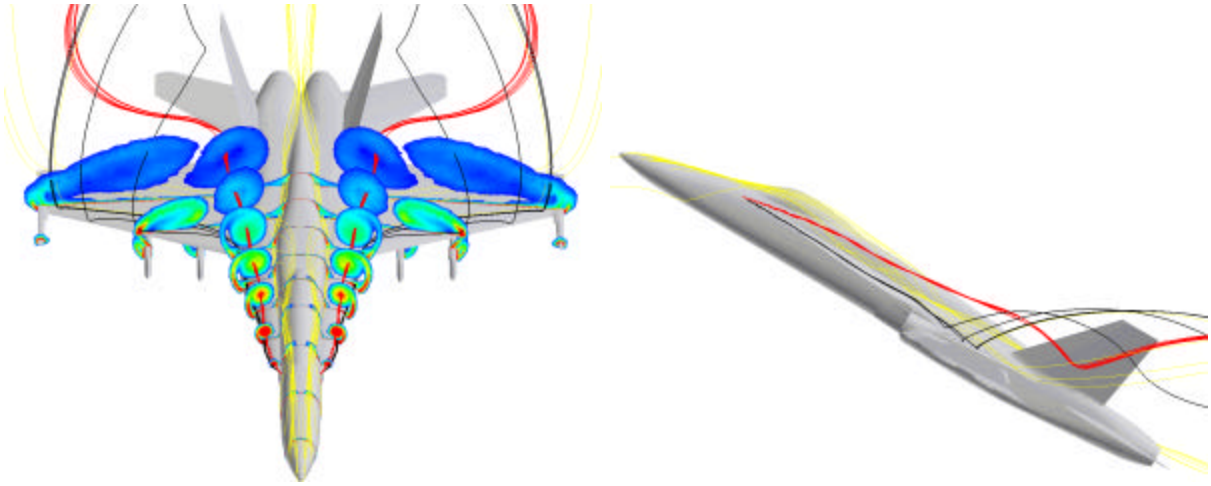

Figure 12. F-18C at 30^{o} angle of attack. Surface cuts on top view are of vorticity magnitude. Red streamlines represent lex vortices, black streamlines represent secondary lex vortex, and yellow streamlines represent forebody vortices.

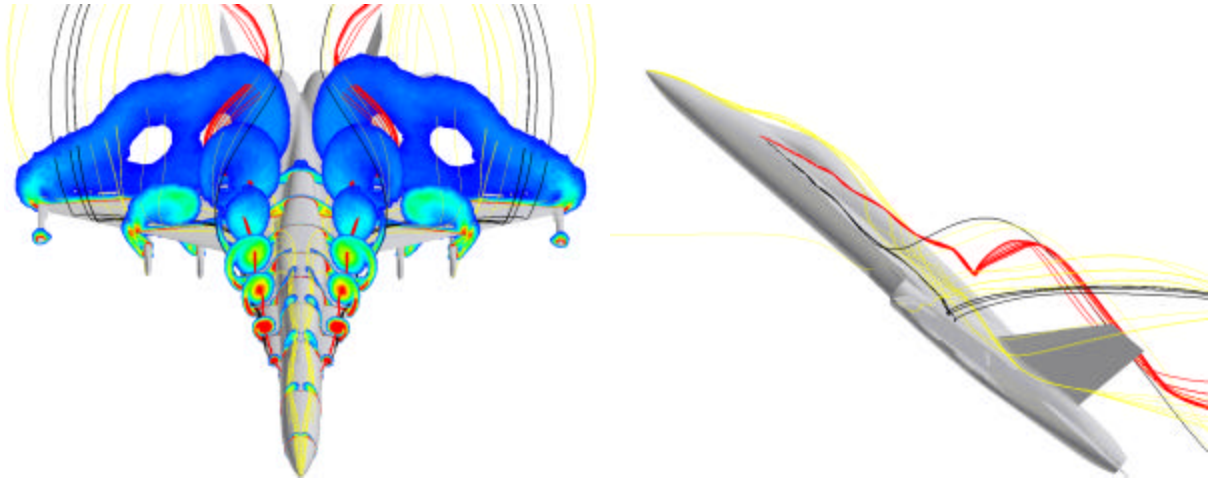

Figure 13. F-18C at 40^{o} angle of attack. Surface cuts on top view are of vorticity magnitude. Red streamlines represent lex vortices, black streamlines represent secondary lex vortex, and yellow streamlines represent forebody vortices.

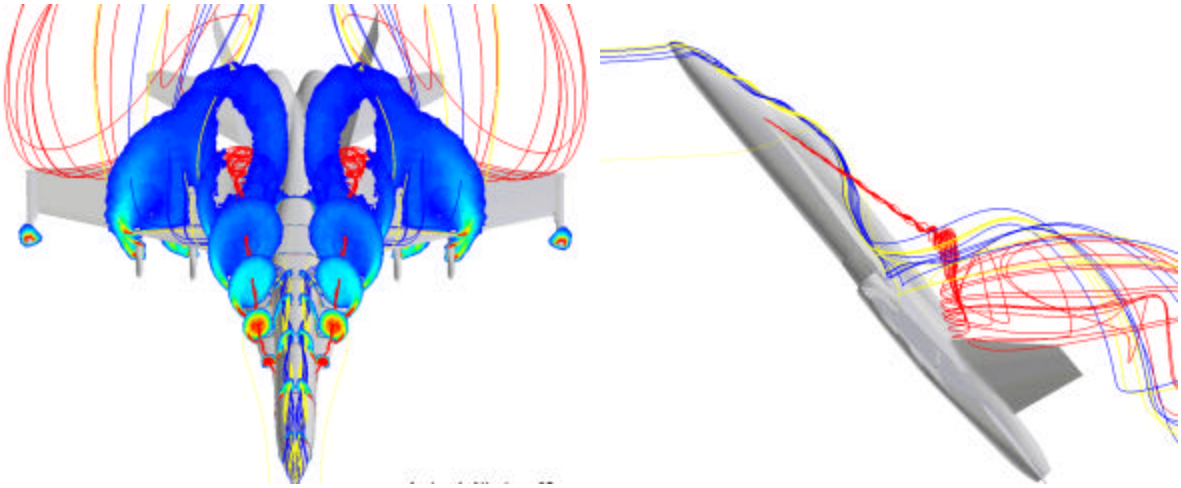

Figure 14. F-18C at 50^{o} angle of attack. Surface cuts on top view are of vorticity magnitude. Red streamlines represent lex vortices and blue/yellow streamlines represent forebody vortices.

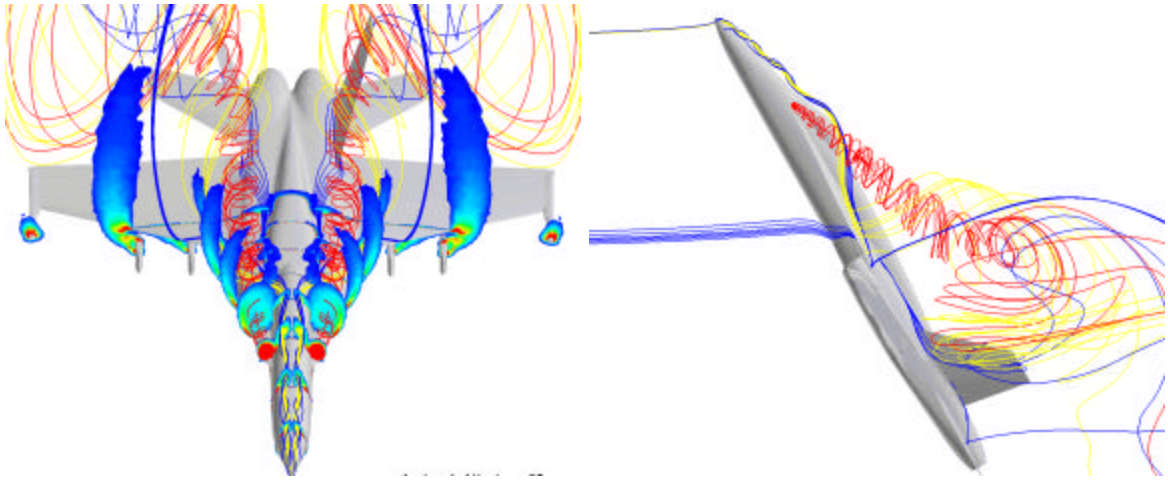

Figure 15. F-18C at 60^{o} angle of attack. Surface cuts on top view are of vorticity magnitude. Red streamlines represent lex vortices and blue/yellow streamlines represent forebody vortices.